Desalination and Water Treatment
www.deswater.com

doi: 10.5004/dwt.2022.28752

269 (2022) 176–187
September

Removal of aqueous lead ions by iron ore tailings/straw biochar composite and its underlying sorption mechanism

Yongliang Chen[a,b,*], Ling Wang[a], Masud Hassan[c,d], Yanju Liu[c,d], Xuedong Wang[b,e], Dajun Ren[a]

[a]*College of Resources and Environmental Engineering, Wuhan University of Science and Technology, Wuhan 430081, China, emails: chenyongliang@wust.edu.cn (Y. Chen), wl1525194807@outlook.com (L. Wang), rendajun@wust.edu.cn (D. Ren)*
[b]*State Environmental Protection Key Laboratory of Mineral Metallurgical Resources Utilization and Pollution Control, Wuhan University of Science and Technology, Wuhan 430081, China, email: xdwang@cnu.edu.cn (X. Wang)*
[c]*Global Centre for Environmental Remediation, College of Engineering, Science and Environment, University of Newcastle, Callaghan, NSW 2308, Australia, emails: Masud.Hassan@uon.edu.au (M. Hassan), Yanju.liu@newcastle.edu.au (Y. Liu)*
[d]*Cooperative Research Centre for Contamination Assessment and Remediation of the Environment (CRC CARE), Callaghan, NSW 2308, Australia*
[e]*College of Resource Environment and Tourism, Capital Normal University, Beijing 100048, China*

Received 27 January 2022; Accepted 14 July 2022

ABSTRACT

A composite material was prepared from iron tailings and straw biochar for lead (Pb) removal from aqueous solution. Microscopic analysis revealed that the surface area of the composite was 131.84 m^2/g and the porosity was predominantly an irregular mesoporous structure (~3.65 nm) in size, and the predominant mineral phases were identified as quartz, magnetite and calcite. The effects of solution pH, adsorbent dosage, contact time, initial sorbate concentration, and temperature on lead(II) removal were investigated. The results showed that the composite could remove 97.05% of lead(II), where solution pH was 5.0, adsorbent dosage was 1.00 g/L, and initial lead(II) concentration was 200 mg/L. The adsorption fitted well to the Langmuir isotherm model, demonstrated monolayer formation of lead ions onto the adsorbent, and the theoretical maximum adsorption capacity of lead(II) was 330.03 mg/g. Adsorption kinetics and thermodynamic indicated that the adsorption reaction was spontaneous and mainly controlled by chemisorption due to presence of abundance of oxygen-containing functional groups and active sites derived from straw and iron ore tailings could bond with lead(II), and columnar cerussite crystals from the reaction between Pb^{2+} and CO_3^{2-} released from the materials were fixed the surface and inside of the materials, improved lead(II) adsorption.

Keywords: Iron tailings; Straw biomass; Composite materials; Biochar; Lead; Adsorption

1. Introduction

Surface water is frequently polluted with heavy metals due to rapid development of industrialization, which seriously threatens biotic and abiotic ecosystems [1,2]. Lead is one of the toxic bio-accumulative heavy metals that generally exists in the environment in a divalent oxidation state, and mainly generated from the industries of lead storage batteries, electroplating, and petroleum processing [3]. Lead contaminated wastewater must be effectively treated

* Corresponding author.

to meet the permissible limits before being discharged into natural water bodies.

At present, the common methods for treating lead contaminated wastewater include chemical precipitation, membrane separation, ion-exchange, electrolysis, and adsorption [4]. Adsorption has been considered a promising technology for the removal of contaminants in wastewater [5–7]. Wide range of adsorbents including activated carbon (AC), biochar, graphene, hydrogel, industrial waste, clay, and nanomaterials, etc. were investigated for removal of organic and inorganic contaminants, including heavy metals ions [8–10]. Of these, various types of biochar with porous structures derived from agricultural waste considered as copious supply, easy accessibilities, and low-cost adsorbents aroused wide attention [4,11]. Several studies have reported that biochar and its composite can be a suitable candidate for removal of heavy metal ions [12–14]. Wang et al. [15] found high sorption ability of pecan biochar to adsorb Pb(II), Cu(II), and Cd(II) with maximum sorption capacities of 153.1, 34.2, and 28.1 mg/g, respectively. Mohammadabadi and Javanbakht [16] used treated waste biomass/alginate adsorbent to adsorb lead(II) in water, and achieved maximum experimental adsorption capacity of 206.75 mg/g. Feedstock sources plays a significant role in the removal of heavy metal ions [17], it has been reported that straw-derived biochar promoted higher lead adsorption due to the micropore properties, oxygen-containing functional groups, and silicon-containing active sites of straw [18–20].

Iron ore tailings are waste generated during the process of iron ore extraction and processing and are usually discharged into the tailings dam to form stockpiles [21]. Owing to the low utilization rate of the tailings and continuous operation of iron ore processing, the tailings dam normally has high carbon footprint and could cause adverse environmental impacts on soil, water, and air [21]. As a result, the recovery and utilization of tailings have received considerable attention. Currently, iron ore tailings are mainly used for the recovery of valuable metals, preparation of building materials, and applications for the treatment of sewage [22]. In addition, tailings can be recycled and reused as a clay substitute because they are mainly composed of inorganic substances such as Si, Al, Ca, Fe, Mg, etc., almost similar to the chemical composition of clay [23]. Iron ore has been confirmed to have a certain adsorption capacity for heavy metal ions [24]. However, reports on the iron ore tailings for metal removal are limited in the existing literature.

By exploiting the complementary advantages of iron ore tailings and waste straw as inorganic and organic adsorbents, respectively, the present study prepared a composite adsorbent using iron ore tailings and waste straw as raw materials by pyrolysis and acid-base activation. The role of surface functional groups and metal-based active sites for the removal of lead ions was critically analyzed. The efficiency of the prepared material to adsorb aqueous lead(II) was probed against solution pH, adsorbent dosage, contact time, and adsorbate initial concentration. The adsorption behavior of the prepared composite material was analyzed by kinetic, isotherm, and thermodynamics models. The adsorption mechanism was investigated by X-ray diffraction (XRD), scanning electron microscope (SEM) and Fourier-transform infrared spectroscopy (FTIR) analysis. This study provided a fundamental understanding for lead removal mechanism of organic and inorganic composite material.

2. Materials and methods

2.1. Raw materials and reagents

The iron tailings were collected from the tailings pond of the iron ore concentrator in Daye City, Hubei Province, China. It contained high Fe content (52.52% Fe_2O_3), along with 21.02% SiO_2, 5.09% MgO, 2.41% CaO, and 2.00% Al_2O_3 (Table 1). The straw was collected from Lianyungang City, Jiangsu Province, China. The straw usually predominantly comprises cellulose, hemicellulose, lignin, and the minerals ash with high silica content [25,26]. Both the iron tailings and straw were respectively dried, ground, and screened to a particle size of <0.074 mm for subsequent use. All the chemicals used, such as $Pb(NO_3)_2$, HNO_3, NaOH, KOH, and HCl, were of analytical grade and purchased from Sinopharm Chemical Reagent Co., Ltd., China. A 1,000 mg/L stock was prepared for the lead(II) sorption study, and deionized (DI) water (18.2 MΩ cm) was used in all the experiments.

2.2. Preparation of composite material

Iron tailings/straw composite material was synthesized by two-step modification methods for the removal of lead ions from lead-contaminated water. Fig. 1 shows the preparation of iron tailings/straw composite adsorption material. Firstly, the pretreated iron tailings (30 g) and straw (10 g) were mixed at a mass ratio of 3:1, then the mixture was immersed in 200 mL of 0.5 mol/L KOH solution at a liquid: solid mass ratio of 5:1 and blended at 150 rpm for 24 h over a magnetic stirrer at 25°C for the first step alkali activation. Subsequently, the suspension liquid was centrifuged at 120 rpm and dried at 80°C overnight (12 h) to get the dried mixture, and then was pyrolyzed at 500°C for 1 h at a heating rate of 10°C/min in a vacuum tube furnace. Before and during pyrolysis, continuous flow of N_2 gas was maintained to avoid the loss of carbon in the form of CO_2. The pyrolyzed sample was cooled to room temperature and ground and sieved (<0.074 mm) for the next modification, with about 0.5 g of the composite material was immersed into 20 mL of 2 mol/L HNO_3 solution, and stirred in a water bath constant temperature oscillator at 55°C for 3 h. After filtration, 25 mL of 2 mol/L NaOH solution were added to the material and again stirred for 0.5 h. Finally, the material was filtered through a filter paper (0.45 μm), and washed with DI water until the pH of the filtrate was close to 7, then oven-dried at 80°C overnight to obtain iron tailings/straw composite adsorption material.

2.3. Batch adsorption experiments

In this experiment, 0.05 g of adsorption material was accurately weighed into a series of 250 mL conical flasks, and 100 mL of $Pb(NO_3)_2$ solution with adjusted pH (adjusted by adding either 0.1 mol/L HNO_3 and/or 0.1 mol/L NaOH solution) was added. The flasks mouth

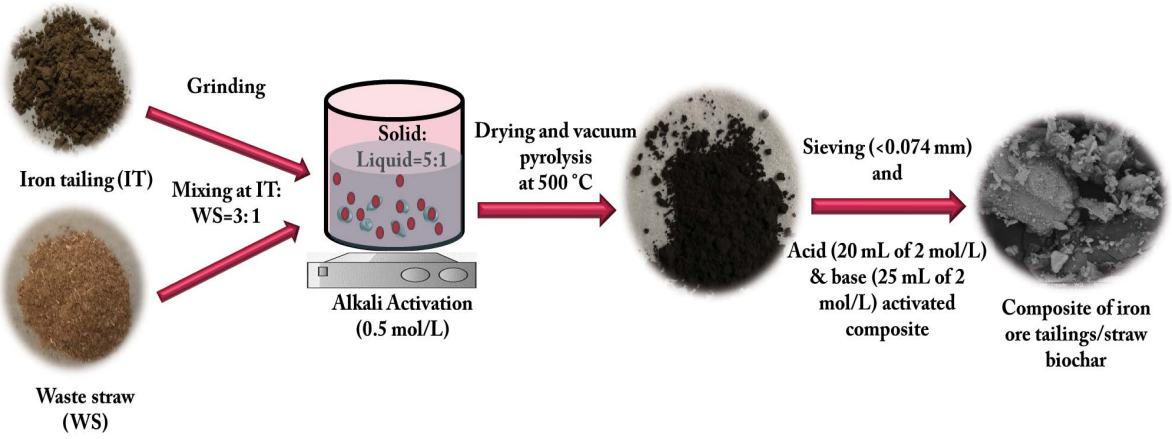

Fig. 1. Preparation flowchart of iron tailings/straw composite adsorption material.

was sealed with polyethylene plastic wrap and placed in an end-over shaker, and oscillated at 200 rpm for adsorption study. After the oscillation and adsorption, supernatant was sampled by a disposable syringe and filtered through a 0.45 μm microporous filter membrane. The filtrate was collected and preserved with a polyethylene plastic tube and the residual concentration of Pb^{2+} in the filtrate was detected by AAS using the method GB/ T7475-87 "Determination of Copper, Zinc, Lead and Cadmium in Water Quality by Atomic Absorption Spectrophotometry".

The influences of solution pH, adsorbent dosage, adsorption kinetics, isotherm, and thermodynamics of lead(II) adsorption by the prepared composite material were examined. The effects of pH on lead(II) adsorption were determined at various solution pH ranging from 2.0 to 7.0 (with contact time (t) = 24 h, temperature (T) = 25°C, initial concentration of lead(II) (C_0) = 200 mg/L, and adsorbent dose (a.d) = 0.5 g/L). The effect of adsorbent dosage was evaluated with different concentrations of adsorbents from 0.25 to 2.0 g/L (with C_0 = 200 mg/L, t = 24 h, T = 25°C, and pH = 5.0). The kinetics study was conducted for up to 24 h of contact time between the adsorbent and adsorbate (with T = 25°C, C_0 = 200 mg/L, pH = 5.0, and a.d = 0.5 g/L). The isotherm study was performed with lead(II) initial concentration ranging from 50 to 800 mg/L (with T = 25°C, t = 24 h, a.d = 0.5 g/L, and pH = 5.0). The adsorption thermodynamics study was conducted at various temperatures of 15°C, 25°C, 35°C, and 45°C (with C_0 = 200 mg/L, t = 24 h, a.d = 0.5 g/L, and pH = 5.0).All experiments were performed in triplicate and average was considered to calculate removal percent as follows:

The lead(II) removal percent (%) and equilibrium adsorption capacity (q_e) in aqueous solution were calculated using the following formulas:

$$\text{Adsorption capacity, } q_e = \frac{(C_0 - C_e)V}{m} \quad (1)$$

$$\text{Removal \%} = \frac{(C_0 - C_e)}{C_0} \times 100 \quad (2)$$

where C_0 is the initial concentration of lead(II) in the solution (mg/L), C_e is the concentration of lead(II) in the solution at equilibrium (mg/L), V is the volume of lead(II)-containing solution (L), and m is the mass of adsorbent (g).

2.4. Characterization of the composite material

In this study, the chemical composition of the iron tailings was examined by X-ray fluorescence Spectrometer (XRF, ZSX Primus, Japan). The residual concentrations of lead(II) after sorption were determined by flame atomic absorption spectrophotometer (FAAS, novAA350, Jena, Germany). The specific surface area of the composite was characterized by automatic surface area and porosity analyzer (ASAP2020, Mcromeritics, USA). The mineral composition of the composite before and after adsorption was determined by XRD (SmartLab SE, Japan). The scanning regions were between 2θ values of 10°~90° at a scanning speed of 0.02°/s. The surface chemical bonds and functional groups of the composite before and after adsorption were measured by FTIR (Vertex70, Bruker, Germany) in the wavelength range of 400~4,000 cm^{-1}. The surface morphology of the composite (A small amount of powder samples were placed on the conductive adhesive on the surface of the copper plate, and the samples were sprayed with gold under the accelerating voltage of 20 kV) was tested by SEM (Apreo S Hivac, America).

3. Results and discussion

3.1. Microscopic properties of the adsorbent

The BET surface area and pore size distribution of the developed composite adsorbent were analyzed (Fig. 2). By following the classification recommended by the International Union of Pure and Applied Chemistry (IUPAC), the composite showed a typical N_2 adsorption and desorption isotherm with type IV isotherm and H3-type hysteresis loop for aggregates of plate-like particles producing slit-shaped pores, indicating the presence of many irregular pore structures in the adsorption materials [27–29]. As can be seen from Fig. 2b, the pore

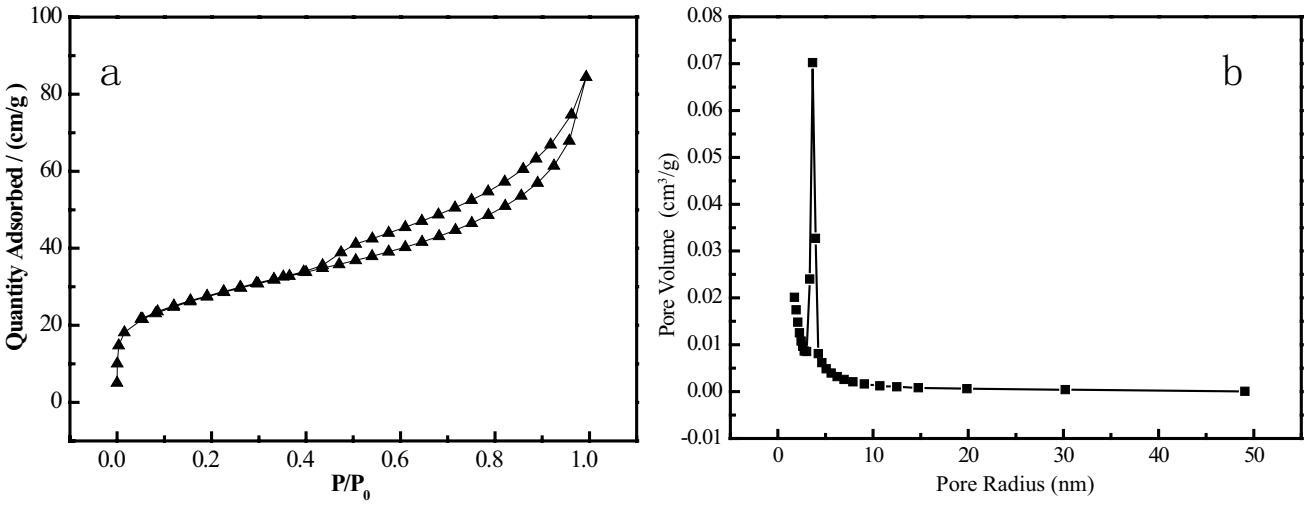

Fig. 2. Adsorption isotherm of N_2 (a) and pore-size distribution curve (b) of the developed adsorbent.

size of the adsorbent is predominantly about 3.65 nm, which is in the range of mesoporous size (2–50 nm), and therefore, the developed composite can be classified as a mesoporous adsorbent material [30,31]. It must be noted that the ionic radius of lead(II) is 0.119 nm [32], thus mesoporous adsorbents are suitable for infiltration and diffusion of the metal ions. The specific surface area (S_{BET}) of the prepared composite was estimated to be 131.84 m^2/g mesoporous structure and large specific surface area generated more active sites both on the surface and inside of the material, resulting in more effective removal of lead(II) from the solution. Hence, the high specific surface area and irregular mesoporous structure distribution might play significant roles in lead(II) adsorption.

Fig. 3a and b show the SEM images of the composite adsorbent before lead(II) adsorption. It can be seen from the picture that the surface of the adsorbent is uneven, and there are some thin flaky, and granular substances (Fig. 3a and b). Combined with the XRD results (Fig. 6), it can be inferred that it is magnetite and quartz.

3.2. Effect of solution pH on lead(II) adsorption

Solution pH is an important factor affecting the adsorption efficiency of the adsorbent. It not only affects the form of heavy metal ions in an aqueous solution but also influences the surface charge of the adsorbent and ionization degree of the adsorbate during the reaction [33,34]. Fig. 4a shows that the removal percent of lead(II) increase with the increasing pH. The removal percent of lead(II) is only 7.5% at pH 2.0, but increase to 90.90% when the pH is up to 7.0.

These effects of pH on lead(II) adsorption could be owing to the change in the surface charge of the adsorbent and the form of Lead ion in the solution. Under highly acidic conditions, a large amount of H^+ existed in the solution, which competed with lead(II) for limited adsorption active sites on the surface of the adsorbent [35]. At the same time, excess H^+ in the solution resulted in protonation of some active groups on the adsorbent surface to form positively charged groups, which repelled positively charged lead(II), thus significantly inhibiting lead(II) adsorption by the adsorbent [36] and resulting in very low lead(II) removal percent. With further increase in pH, the highly acidic condition gradually turned into weakly acidic condition, the H^+ concentration in the solution decreased, and the active group deprotonated with a negative charge. Consequently, the lead(II) adsorption sites on the adsorbent increased [34], enhancing the lead(II) adsorption capacity and removal percent. In addition, the forms of lead ions varied with the pH of the solution. When the solution pH was <5.5, lead in the solution occurred mainly as lead(II). However, when the solution pH was >5.5, hydroxyl coordination ions of lead gradually formed and began to precipitate [37,38]. Besides, white precipitates of $Pb(OH)_2$ gradually appeared in the solution at pH 6.0 and 7.0. Therefore, the initial pH of the solution was controlled at 5 in the subsequent experiments to accurately study the lead(II) adsorption characteristics onto the composite.

3.3. Effect of adsorbent dosage on lead(II) adsorption

With the gradual increased in adsorbent dosage from 0.25 to 2.00 g/L, the removal percent of lead(II) by the composite material linearly increased at first and then became stable, whereas the adsorption capacity persistently decreased (Fig. 4b). When the adsorbent dosage was increased from 0.25 to 1.00 g/L, the removal percent of lead(II) increased from 32.08% to 97.05%, and the adsorption capacity decreased from 252.50 to 190.98 mg/g. With a further increased the adsorbent dosage to 2.00 g/L, the lead(II) removal percent slightly increased to 98%, whereas the adsorption capacity continued to decrease to 97.09 mg/g. The increase in the initial lead(II) removal percent could be attributed to the increase in the adsorption dosage, which provided more active sites for lead(II) adsorption. However, lead(II) removal percent slightly changed with further increase in the adsorbent dosage because of saturation of adsorption. The reason for the persistent decrease in the adsorption capacity with increasing adsorbent dosage was owing to a relative decrease in the amount of

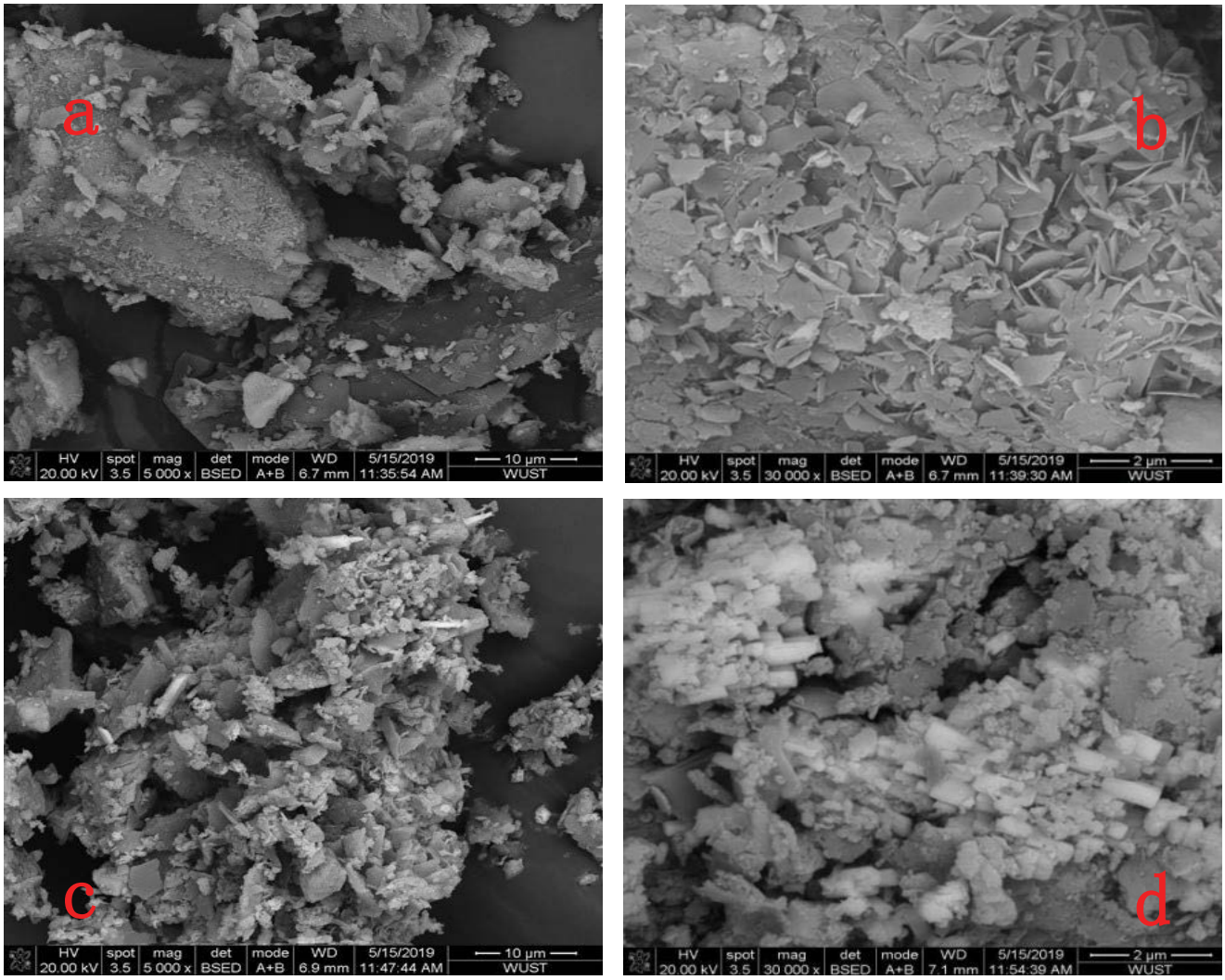

Fig. 3. SEM images of the composite material before (a and b) and after (c and d) lead(II) adsorption.

adsorbed lead(II) per unit of adsorbent, or the decrease in the active sites resulting from the aggregation of the adsorbent [31,39]. Considering the lead(II) removal percent and adsorption capacity, 1.00 g/L composite adsorbent could effectively remove lead(II) from wastewater, with 97.05% lead(II) removal percent and 190.98 mg/g adsorption capacity, respectively.

3.4. Effect of contact time on lead(II) adsorption and adsorption kinetics

Fig. 4c indicates the change in lead(II) adsorption capacity of the developed composite material with contact time. It can be seen from the figure that the lead(II) adsorption capacity of the adsorbent rapidly increased with the extension of contact time in the initial stage (0–4 h), and then slowly increased to reach adsorption saturation at 12 h. As the adsorption of lead(II) mainly occurred on the surface of the composite and on some macropores, and lead(II) was quickly adsorbed in the initial stage, the adsorption rate was relatively higher. However, as the adsorption progressed, lead(II) was gradually adsorbed onto the microporous structure of the material and the lead(II) mass transfer rate in the micropores was relatively slow. Hence,

Table 1
Chemical composition of iron tailings (wt.%)

Material	Iron tailings
SiO_2	21.02
Al_2O_3	2.00
Fe_2O_3	52.52
CaO	2.41
MgO	5.09
K_2O	0.28
Na_2O	0.59
TiO_2	0.04
LOI	15.99

LOI: loss on ignition.

lead(II) adsorption percent slowly decreased with the extension of contact time until the adsorption equilibrium was achieved at 12 h, with the lead(II) adsorption capacity of the adsorbent at equilibrium reaching 250.17 mg/g.

Adsorption kinetic modeling is used to describe the transfer of lead(II) from the solution to the solid adsorbent [40]. The parameters of adsorption kinetic model are shown in Table 2. In the present study, pseudo-first-order and pseudo-second-order kinetic models were employed to fit the experimental data and analyze the adsorption processes as follows:

Adsorption kinetic models:

Nonlinear form of the pseudo-first-order kinetic equation:

$$q_t = q_e\left(1 - e^{-k_1 t}\right) \tag{3}$$

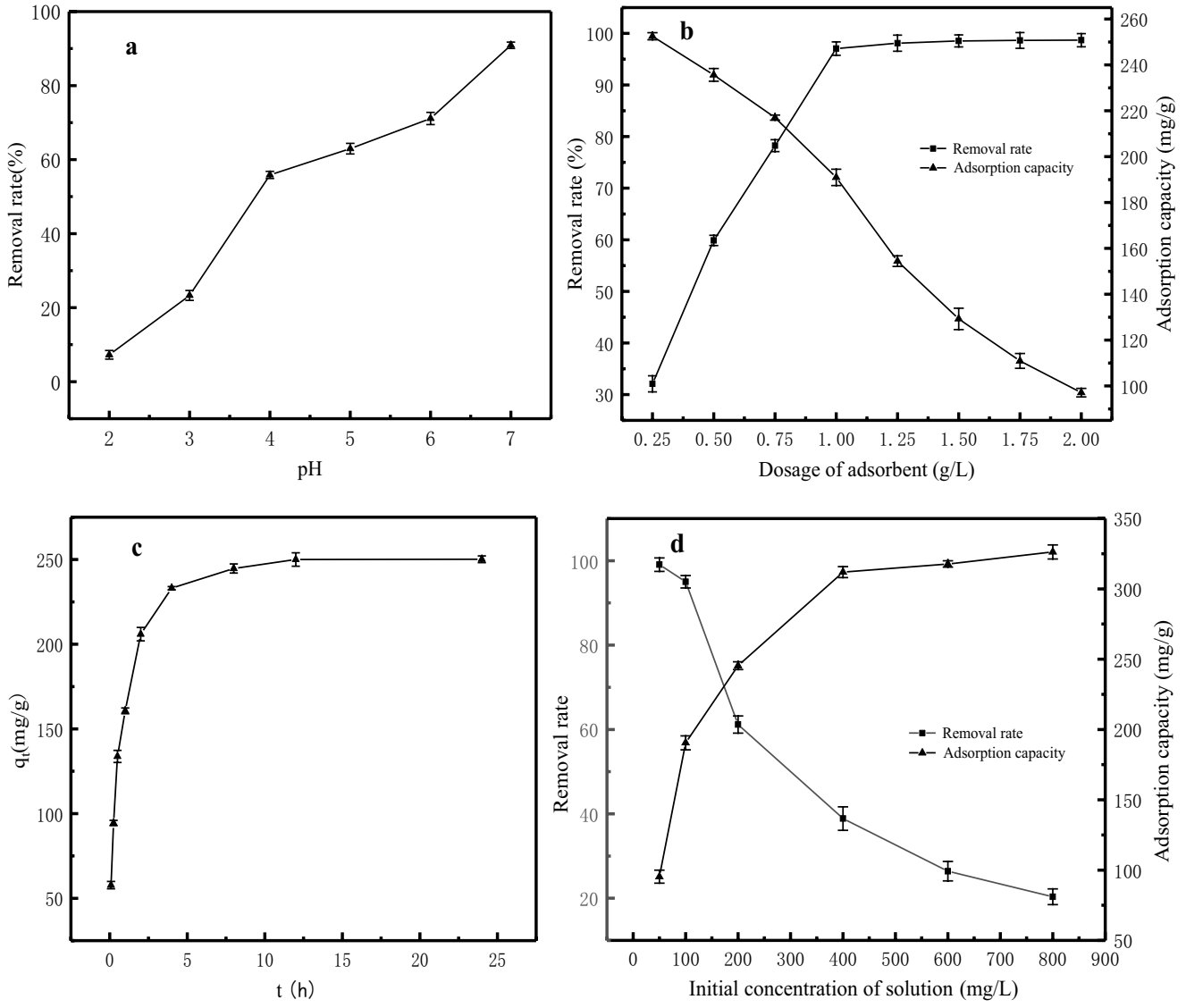

Fig. 4. Effects of solution pH (a), adsorbent dosage (b), contact time (c), initial lead(II) concentration (d) on lead(II) adsorption.

Table 2
Relevant parameters of adsorption isothermal model and adsorption kinetic model

Langmuir isotherm adsorption model			Freundlich isotherm adsorption model			Pseudo-first-order kinetic model			Pseudo-second-order kinetic model		
K_L	q_m	R^2	K_F	$1/n$	R^2	q_e	k_1	R^2	q_e	k_2	R^2
0.0805	330.03	0.9989	105.8264	0.1858	0.8515	238.97	0.0252	0.9268	255.58	0.0001	0.9855

Nonlinear form of the pseudo-second-order kinetic equation:

$$q_t = \frac{k_2 q_e^2 t}{1 + k_2 q_e t} \tag{4}$$

where t is the contact time (min), q_t and q_e are the amounts of lead(II) adsorbed onto the adsorbent at time t and equilibrium, respectively (mg/g), and k_1 (min^{-1}) and k_2 (g mg^{-1} min^{-1}) are the pseudo-first-order and pseudo-second-order model rate constants, respectively. The fitting results are shown in Fig. 5.

It can be observed from Fig. 5 that the pseudo-second-order model is associated with higher correlation coefficients (R^2; 0.9855) than the pseudo-first-order kinetics model (R^2; 0.9268), suggesting that it better described the adsorption process than the pseudo-first-order model. Both physical adsorption and chemical adsorption existed in the adsorption process of lead ions at the same time. The physical adsorption of lead by the composite was mainly realized through electrostatic interaction. Based on pseudo-second-order kinetic model assumptions, the reaction rate is proportional to the number of active sites on the surface of the adsorbent, and the rate-limiting step may be a chemical adsorption between the adsorbate and the adsorbent, namely the chemical interaction between the lead ions in the aqueous medium and the functional groups on the surface of the composite [41,42]. The fitting results show that lead(II) adsorption onto the composite is mainly controlled by chemical adsorption and involves electron sharing or electron transfer between the adsorbent and adsorbate. Lead(II) adsorption capacity onto the composite at equilibrium is 255.58 mg/g, which is close to the actual experimental value (Fig. 4c).

3.5. Effect of initial lead(II) concentration on lead(II) adsorption and adsorption isotherm

The adsorption isotherm refers to the relationship of the concentration of solute molecules between the two phases when the adsorption process reaches equilibrium at a two-phase interface at a certain temperature. In the present study, the adsorption equilibrium of lead(II) in solution was described using the Langmuir and Freundlich isotherm models, and their linear equations can be given as follows:

$$\text{Langmuir model}: \frac{C_e}{q_e} = \frac{1}{K_L q_m} + \frac{C_e}{q_m} \tag{5}$$

$$\text{Freundlich model}: \ln q_e = \ln K_F + \frac{1}{n} \ln C_e \tag{6}$$

where q_e (mg/g) and q_m (mg/g) are the lead(II) adsorption capacity at equilibrium and the theoretical maximum adsorption capacity (mg/g), respectively; C_e is the concentration of the adsorbate at equilibrium (mg/g); K_L and K_F represent the reaction rate constant in the isotherm model; n is the Freundlich linearity constant used to evaluate the lead(II) concentration nonlinearity degree between the solution and adsorbent.

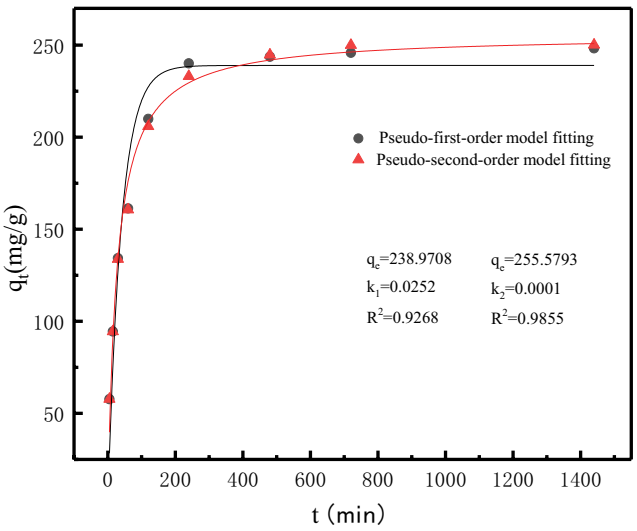

Fig. 5. Kinetics of lead(II) adsorption onto the composite adsorbent.

The effect of initial concentration on lead(II) adsorption onto the composite at 25°C is given in Fig. 4d and the relevant isotherm modeling parameters are presented in Table 2. As shown in Fig. 4d, with the increase in the initial lead(II) concentration from 50 to 800 mg/L, lead(II) removal % of the composite gradually decrease, whereas the adsorption capacity slowly increase and then remain stable, indicating the attainment of equilibrium, with the saturated adsorption capacity of 326.25 mg/g. It can be observed from Table 2 that the R^2 is higher for the Langmuir model than that for the Freundlich isotherm model, implying that the Langmuir model can better describe the adsorption process. Moreover, the results reveal that monolayer physisorption or chemisorption process played a major role in lead(II) adsorption, and that some chemical interactions might be involved. The theoretical maximum adsorption capacity q_m is 330.03 mg/g, which is close to the measured value (Fig. 4d). Furthermore, when compared with previous studies, the adsorption effects determined in the present study are better [14,43–45]. In the Freundlich model, the $1/n$ is <1 (adsorption constant $1/n$ is 0.1858), representing heterogeneity of the adsorbent [46,47]. The adsorbent is highly heterogeneous due to its versatile counterpart.

3.6. Adsorption thermodynamics

The thermodynamics of lead(II) adsorption onto the developed composite material was investigated to explore the adsorption behavior. The thermodynamics parameters of Gibbs free energy were used to determine the probability of the adsorption process, and were calculated as follows:

$$K_d = \frac{q_e}{C_e} \tag{7}$$

$$\Delta G^\circ = \Delta G^\circ - T\Delta S^\circ \tag{8}$$

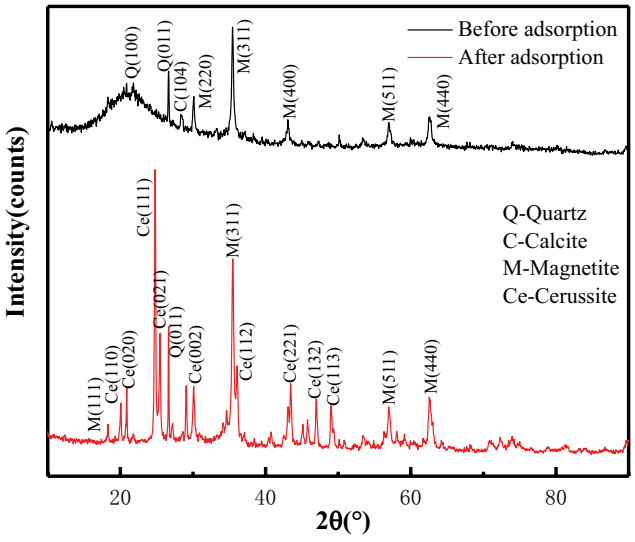

Fig. 6. XRD patterns of the composite material before and after lead(II) adsorption.

$$\ln K_d = -\frac{\Delta H^\circ}{(RT)} + \frac{\Delta S^\circ}{R} \tag{9}$$

where K_d is the equilibrium constant (mL/g), q_e is the adsorption capacity at equilibrium, C_e is the concentration of the adsorbate at equilibrium (mg/L), R is the universal gas constant (8.314 J/(mol K)), and T is the system temperature (K).

The adsorption thermodynamics fitting results and parameters are shown in Table 3. It can be observed from the table that the values of Gibbs free energy ΔG° change for the prepared composite material are negative at different temperatures, indicating that the process of lead(II) adsorption onto the composite is spontaneous under experimental conditions. The change of Gibbs free energy decreases with increasing temperatures, revealing that the temperature rise is beneficial to spontaneous adsorption reaction. The adsorption enthalpy ΔH° of lead(II) on the composite adsorbent is 16.1244 kJ/mol, which demonstrate that lead(II) adsorption onto the composite is an endothermic process, and that high temperature is conducive to the adsorption reaction [48]. Furthermore, the reaction entropy change (ΔS°) is 64.2917 J/(mol K), implying that lead(II) adsorption onto the developed material is highly random. Thus, it could be concluded that lead(II) adsorption onto the developed composite is spontaneous and endothermic, and that the increase in temperature is beneficial to the adsorption of lead(II) from wastewater.

3.7. Comparative evaluation of lead(II) adsorption

Previous studies reported lead(II) sorption by hydrogel, biochar, graphene oxide, clay mineral, polymer, and iron-based nanomaterials [29,49,50]. Table 4 highlighted some of the recent results from the literature, including our present study for comparative evaluation of the sorption performance for lead(II) removal. Of these, biochar and activated carbon were widely used to remove lead ions due to their low production cost [51–53]. Cechinel et al. [54] adsorbed lead(II) with commercially available activated carbon, and the theoretical maximum adsorption capacity was much lower than biochar. Among all kinds of biochar, straw-derived biochar performed well for lead removal [55]. It has been also reported that, higher temperature pyrolyzed biochar had higher sorption performance than the lower temperature pyrolyzed biochar [18,56]. Graphene and CNT had lower sorption capacity for lead removal due to higher hydrophobicity and lack of oxygen-containing active sites. For example, Li et al. [57] adsorbed lead(II) with carbon nanotubes, the theoretical maximum adsorption capacity was 49.95 mg/g and the lead removal percent was 87.8%.

Table 3
Thermodynamics parameters of lead(II) adsorption onto the developed composite

T (K)	ΔH° (kJ/mol)	ΔS° [J/(mol K)]	ΔG° (kJ/mol)
288.15	16.1244	64.2917	–2.4013
298.15			–3.0442
308.15			–3.6871
318.15			–4.3300

Although, iron nanoparticle has higher sorption capacity, it is unable to remove lead ions completely from wastewater due to lack of selectivity. For example, Chen et al. [58] adsorbed lead(II) with iron oxide nanomaterials with cobalt and nickel doping at the same temperature, the study reported that the theoretical maximum adsorption capacities of Fe_2O_3, Co-Fe_2O_3 and Ni-Fe_2O_3 were 93.90, 136.00 and 97.53 mg/g, respectively, and the percentage of lead(II) removal by Fe_2O_3, Co-Fe_2O_3, and Ni-Fe_2O_3 were reached 86.0%, 94.5%, and 91.1% respectively. Similarly, Chen et al. [59] and Shi et al. [60] used metal nanomaterials to adsorb lead(II) and achieved good results. Although metal bi/trimetallic nanoparticles had higher sorption capacity, the cost of these nanoparticles is considerably higher. In this study, iron tailings/straw composite as a readily available and low-cost waste material was used to adsorb lead(II), the theoretical maximum adsorption capacity was 330.03 mg/g and the maximum removal percent was 97.05%, which is competitive enough in comparison to existing report. Thus, it can be concluded that the composite has certain advantages and significance in the treatment of lead ions from wastewater.

4. Adsorption mechanism

In order to understand the sorption mechanism in more details, XRD and FTIR analyses for the composite before and after lead(II) adsorption were performed. The XRD patterns of the composite before and after lead(II) adsorption are shown in Fig. 6. The mineral phases of the composite before adsorption were magnetite (JCPDS 99-0073), quartz (JCPDS 99-0088), and calcite (JCPDS 99-0022), which predominantly originated from the iron tailings composed of Fe_3O_4, SiO_2, and $CaCO_3$ (Table 1).

Table 4
Comparison of lead(II) adsorption onto different adsorbents

Adsorbents	Pollutants	Model fitting	Sorption mechanism	Sorption capacity (mg/g)	References
Activated carbon	Pb	Elovich model	\	50.20	[49]
Rice husk biochars	Pb	F, PSO	Precipitation: forming pyromorphite solidified lead	26.70	[56]
Microwave-pyrolyzed biochars	Pb	F, PSO	Precipitation as hydrocerussite and lead oxide phosphate; surface complexation and cation–π interaction	165.00	[53]
Magnetically modified biochars	Pb	\	Cation exchange; metal sorption	179.00	[54]
Rice straw biochars	Pb	L, F, PSO	Precipitation: the formation of lead oxalate for RSB300 and hydrocerussite for RSB500 and RSB700	127.00–198.00	[18]
Mesoporous biopolymer beads	Pb	L, PSO	Pore-filling, ion-exchange, and electrostatic interaction	26.49 ± 2.04	[31]
CNTs	Pb	L, F	Surface functional groups; ion-exchange	49.95	[57]
Co-Fe_2O_3	Pb	PFO, F	Multilayer coverage and chemisorption	136.00	[58]
Ni-Fe_2O_3	Pb	PFO, F	Multilayer coverage and chemisorption	97.53	[58]
Sulfonated Fe_3O_4 NPs	Pb	L, PSO	Complexation reaction of sulfo group	108. 93	[59]
Fe_2O_3	Pb	PFO, L	Monolayer coverage and chemisorption	93.90	[58]
Magnetic biochar	Pb	L, PSO	Electrostatic interaction; surface complexation; ion-exchange; direct reduction by nZVI	206.50	[52]
Activated carbon	Pb	PSO, L	Cation exchange; electrostatic repulsion	47.62	[51]
Cu-MOFs/Fe_3O_4	Pb	F, PSO	Chemical bonding with N of the ligands	219.00	[60]
Iron ore tailing/straw biochar	Pb	L, PSO	Precipitation; chemical interaction	330.03	This study

PSO: pseudo-second-order kinetic model; PFO: pseudo-first-order kinetic model; L: Langmuir isotherm adsorption model; F: Freundlich isotherm adsorption model.

Besides, an obvious amorphous diffraction hump existed in the range of 2θ from 15° to 25°, which indicated the presence of organic amorphous biochar from straw pyrolysis [28,61]. However, after lead(II) adsorption, many new cerussite ($PbCO_3$) (JCPDS 99-0026) could be observed in the composite. The main characteristic peaks at approximately 24.8°, 25.5°, and 43.5° were corresponding to the diffraction from the (111), (021) and (221) planes of $PbCO_3$, and other weaker diffraction peaks at 2θ = 20°, 20.9°, 29°, 35.6°, 47° and 49° can be indexed as the (110), (020), (002), (112), (132) and (113) planes. The characteristic peaks of calcite in the material disappeared, and the main mineral phases were quartz, magnetite, and $PbCO_3$. The alteration in the XRD pattern might be owing to calcite dissolution to release CO_3^{2-}, which in turn reacted with lead(II) to form new crystalline $PbCO_3$ during the adsorption process, facilitating lead(II) immobilization in the solution.

It can be seen from Fig. 3c and d that after lead(II) adsorption onto the composite, expect for the thin and granular particles, some columnar crystals were formed on the surface and in the irregular pores of the composite, which confirmed that cerussite ($PbCO_3$) precipitate was formed resulting from the reaction between lead(II) in the solution and CO_3^{2-} released from the mineral components, consistent with the XRD results (Fig. 6).

Fig. 7 shows the FTIR spectra for the composite adsorbent before and after lead(II) adsorption. Some peaks were barely altered, and the peaks at 1,011.76 and 458.50 cm^{-1} could be attributed to the antisymmetric and symmetric tensile vibration of Si–O–Si bonds [38], which was obviously caused by the existence of silicon dioxide. The peak at 567.95 cm^{-1} corresponded to Fe–O vibration [40], which might have resulted from magnetite in the raw materials. The characteristic peaks at 3,784.45; 3,513.22 and 3,302.12 cm^{-1} could correspond to OH groups [62,63], indicating the existence of the hydroxyl groups on the material surface. And their intensities significantly weakened after lead(II) adsorption, which might be owing to the decrease in OH groups as a result of binding with lead ions in the solution.

The peaks at 1,631.08 and 1,434.15 cm^{-1} corresponded to the bending and antisymmetric stretching vibrations of CO_3^{2-} [64]. However, they shifted to 1,669.61 and 1,439.86 cm^{-1} after lead(II) adsorption, respectively, owning to adsorption of lead(II), which was consistent with the results of $PbCO_3$ production in XRD analysis. In other words,

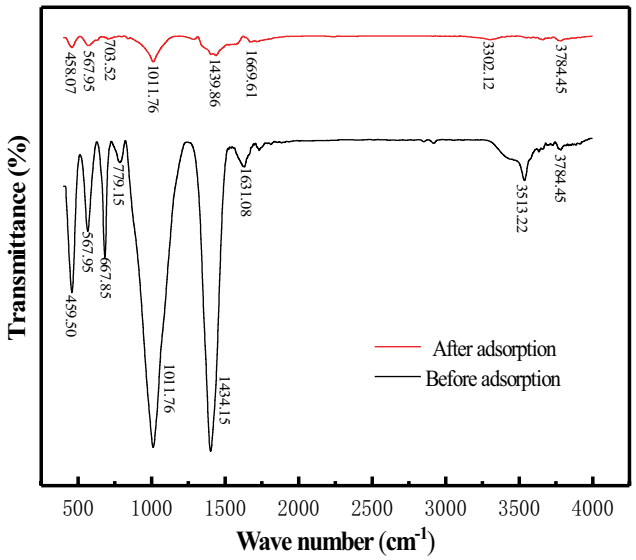

Fig. 7. FTIR spectroscopy of the composite material before and after lead(II) adsorption.

these changes in the position of the bands suggested that the carbonate ions on the surface of the material were involved in the interaction with lead ions [63]. The C–H bending in alkenes (779.15 cm^{-1}) and out-of-plane N–H bending vibrations (667.85 cm^{-1}) gradually disappeared or shifted (704.95 cm^{-1}) after lead(II) adsorption [38], suggesting that aliphatic compounds were highly aromatized during the carbonization process. All these observations suggested that there were different kinds of functional groups on the surface of the adsorption material, and these groups could represent the binding sites for lead ions from aqueous media. This meant that chemical interaction between the lead ions and surface functional groups of the composite played a vital role in lead(II) adsorption.

In conclusion, the sorption mechanism of lead(II) onto the composite could be concluded as Fig. 8, which is similar to the adsorption mechanism of some materials for lead in Table 4. Besides, the high specific surface area and abundant pore structure of the composite were very conducive to the adsorption and immobilization of lead(II), and that the formation of $PbCO_3$ improved the removal of lead(II) from wastewater.

5. Conclusion

In this study, a new composite adsorbent was prepared by pyrolysis and acid–base modification with iron tailings and straw biochar as raw materials for the adsorption of lead(II) in aqueous solution, which developed a new approach for the comprehensive utilization of iron tailings and straw, not only achieved the purpose of "treating waste with waste", but also provided a theoretical basis for its practical application in the field of environmental purification. BET analysis indicated that the composite had large surface area (131.84 m^2/g) and abundant mesopores structure (3.65 nm), providing condition for lead(II) removal. The results showed that the prepared composite exhibited efficient lead(II) adsorption performance in aqueous solution, with a maximum lead(II) removal percent of 97.05%. Langmuir model (R^2: 0.9989) and pseudo-second-order model (R^2: 0.9855) better described the adsorption process, the theoretical maximum adsorption capacity was 330.03 mg/g, which had great advantages over other existing relevant report, demonstrated that with monolayer formation of lead ion through physisorption and chemisorption mechanism, chemosorption being the predominant sorption reaction mechanism for the lead(II) removal. Adsorption thermodynamics analyses revealed that the lead(II) adsorption onto the composite was a spontaneous and endothermic process. Microscopic analysis indicated the formation of cerussite ($PbCO_3$) in the composite material after the adsorption, and the adsorption of lead(II) by the composite material was mainly the result of chemical interaction between lead ions and functional groups on the surface of composites. Lead ions reacted with CO_3^{2-} groups on the surface of materials to form precipitation, which played an important role in the removal of lead(II).

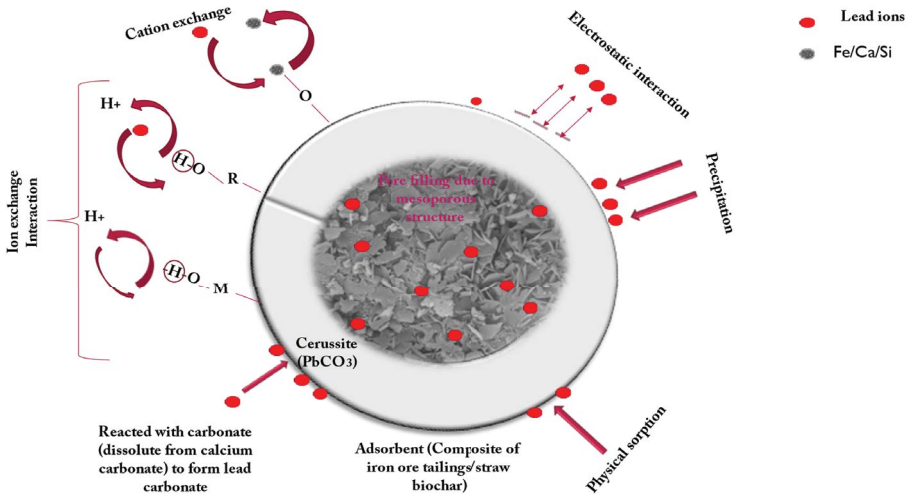

Fig. 8. Adsorption mechanism of lead onto the composite material.

Acknowledgments

This research was supported by the Open Foundation of State Environmental Protection Key Laboratory of Mineral Metallurgical Resources Utilization and Pollution Control (HB201913), Natural Science Foundation of Hubei Province of China (No. ZRMS2018000825), the Science Foundation of Wuhan Science and Technology Planning Project (No. 2020020601012274) and the Hubei Provincial Education Department Projects of Science and Technology Research, (No. Q20141108).

Availability of data

All data generated or analyzed during this study are included in this published article.

Ethics approval

There are no relevant ethical issues to be disclosed in this study.

Data availability

The datasets used and analyzed during the current study are available from the corresponding author on reasonable request.

References

[1] M. Karatas, Removal of Pb(II) from water by natural zeolitic tuff: kinetics and thermodynamics, J. Hazard. Mater., 199 (2012) 383–389.
[2] D. Xu, X.L. Tan, C.L. Chen, X.K. Wang, Adsorption of Pb(II) from aqueous solution to MX-80 bentonite: effect of pH, ionic strength, foreign ions and temperature, Appl. Clay Sci., 41 (2008) 37–46.
[3] X.W. Lu, X.A. Ning, P.H. Lee, K. Shih, F. Wang, E.Y. Zeng, Transformation of hazardous lead into lead ferrite ceramics: crystal structures and their role in lead leaching, J. Hazard. Mater., 336 (2017) 139–145.
[4] S. Babel, T.A. Kurniawan, Low-cost adsorbents for heavy metals uptake from contaminated water: a review, J. Hazard. Mater., 97 (2003) 219–243.
[5] Y. Chammui, P. Sooksamiti, W. Naksata, S. Thiansem, O.A. Arqueropanyo, Removal of arsenic from aqueous solution by adsorption on leonardite, Chem. Eng. J., 240 (2014) 202–210.
[6] F. Wang, Y. Pan, P. Cai, T. Guo, H. Xiao, Single and binary adsorption of heavy metal ions from aqueous solutions using sugarcane cellulose-based adsorbent, Bioresour. Technol., 241 (2017) 482–490.
[7] F. Fu, Q. Wang, Removal of heavy metal ions from wastewaters: a review, J. Environ. Manage., 92 (2011) 407–418.
[8] M. Hassan, R. Naidu, J. Du, Y. Liu, F. Qi, Critical review of magnetic biosorbents: their preparation, application, and regeneration for wastewater treatment, Sci. Total Environ., 702 (2019) 1–22.
[9] A.A. Basaleh, M.H. Al-Malack, T.A. Saleh, Poly(acrylamide acrylic acid)/Baghouse dust magnetic composite hydrogel as an efficient adsorbent for metals and MB; synthesis, characterization, mechanism, and statistical analysis, Sustainable Chem. Pharm., 23 (2021) 1–13.
[10] O.A. Bin-Dahman, T.A. Saleh, Synthesis of polyamide grafted on biosupport as polymeric adsorbents for the removal of dye and metal ions, Biomass Convers. Biorefin., (2022), doi: 10.1007/s13399-022-02382-8.
[11] M.I. Inyang, B. Gao, Y. Yao, Y. Xue, A. Zimmerman, A. Mosa, P. Pullammanappallil, Y.S. Ok, X. Cao, A review of biochar as a low-cost adsorbent for aqueous heavy metal removal, Crit. Rev. Env. Sci. Technol., 46 (2016) 406–433.
[12] L.C.A. Melo, A.P. Puga, A.R. Coscione, L. Beesley, C.A. Abreu, O.A. Camargo, Sorption and desorption of cadmium and zinc in two tropical soils amended with sugarcane-straw-derived biochar, J. Soils Sediments, 16 (2016) 226–234.
[13] S.M. Yakout, E. Elsherif, Biosorption behavior of Sr^{2+} using straw-derived biochar: equilibrium and isotherm study, Desal. Water Treat., 57 (2015) 7262–7269.
[14] B. Li, L. Yang, C.Q. Wang, Q.P. Zhang, Q.C. Liu, Y.D. Li, R. Xiao, Adsorption of Cd(II) from aqueous solutions by rape straw biochar derived from different modification processes, Chemosphere, 175 (2017) 332–340.
[15] H. Wang, B. Gao, S. Wang, J. Fang, Y. Xue, K. Yang, Removal of Pb(II), Cu(II), and Cd(II) from aqueous solutions by biochar derived from $KMnO_4$ treated hickory wood, Bioresour. Technol., 197 (2015) 356–362.
[16] S.I. Mohammadabadi, V. Javanbakht, Fabrication of dual cross-linked spherical treated waste biomass/alginate adsorbent and its potential for efficient removal of lead ions from aqueous solutions, Ind. Crops Prod., 168 (2021) 1–13.
[17] M. Hassan, Y. Liu, R. Naidu, S.J. Parikh, I.R. Willett, Influences of feedstock sources and pyrolysis temperature on the properties of biochar and functionality as adsorbents: a meta-analysis, Sci. Total Environ., 744 (2020) 1–15.
[18] Z. Shen, D. Hou, F. Jin, J. Shi, X. Fan, D.C.W. Tsang, D.S. Alessi, Effect of production temperature on lead removal mechanisms by rice straw biochars, Sci. Total Environ., 655 (2019) 751–758.
[19] H. Gong, J. Chi, Z. Ding, F. Zhang, J. Huang, Removal of lead from two polluted soils by magnetic wheat straw biochars, Ecotoxicol. Environ. Saf., 205 (2020) 1–8.
[20] R. Amen, M. Yaseen, A. Mukhtar, J.J. Klemeš, S. Saqib, S. Ullah, A.G. Al-Sehemi, S. Rafiq, M. Babar, C.L. Fatt, M. Ibrahim, S. Asif, K.S. Qureshi, M.M. Akbar, A. Bokhari, Lead and cadmium removal from wastewater using eco-friendly biochar adsorbent derived from rice husk, wheat straw, and corncob, Cleaner Eng. Technol., 1 (2020) 1–11.
[21] N. Zhang, B. Tang, X.M. Liu, Cementitious activity of iron ore tailing and its utilization in cementitious materials, bricks and concrete, Constr. Build. Mater., 288 (2021) 1–14.
[22] Y.S. Liu, F. Du, L. Yuan, H. Zeng, S.F. Kong, Production of lightweight ceramisite from iron ore tailings and its performance investigation in a biological aerated filter (BAF) reactor, J. Hazard. Mater., 178 (2010) 999–1006.
[23] Y. He, Y. Lv, L. Han, Synthesis and adsorption property of mesoporous molecular sieve MCM-41 from iron ore tailings, Adv. Mater. Res., 92 (2010) 255–262.
[24] K. Wang, B. Xing, Adsorption and desorption of cadmium by goethite pretreated with phosphate, Chemosphere, 48 (2002) 665–670.
[25] V. Balasundram, N. Alias, N. Ibrahim, R.M. Kasmani, H. Hasbullah, Thermal characterization of Malaysian biomass via thermogravimetric analysis, J. Energy Saf. Technol., 1 (2018) 31–38.
[26] I.A. Rahman, J. Ismail, Preparation and characterization of a spherical gel from a low-cost material, J. Mater. Chem., 3 (1993) 931–934.
[27] M. Thommes, K. Kaneko, A.V. Neimark, J.P. Olivier, F. Rodriguez-Reinoso, J. Rouquerol, K.S.W. Sing, Physisorption of gases, with special reference to the evaluation of surface area and pore size distribution (IUPAC Technical Report), Pure Appl. Chem., 87 (2015) 1051–1069.
[28] L.M.M. Machado, S.F. Lütke, D. Perondi, M. Godinho, M.L.S. Oliveira, G.C. Collazzo, G.L. Dotto, Treatment of effluents containing 2-chlorophenol by adsorption onto chemically and physically activated biochars, J. Environ. Chem. Eng., 8 (2020) 1–8.
[29] Z. Tang, P. Gao, Y. Li, Y. Han, W. Li, S. Butt, Y. Zhang, Recovery of iron from hazardous tailings using fluidized roasting coupling technology, Powder Technol., 361 (2020) 591–599.
[30] M. Hassan, A.K. Deb, F. Qi, Y. Liu, M. Hassan, Magnetically separable mesoporous alginate polymer beads assist adequate

removal of aqueous methylene blue over broad solution pH, J. Cleaner Prod., 319 (2021) 1–15.
[31] M. Hassan, Y. Liu, R. Naidu, J. Du, F. Qi, S.W. Donne, M.M. Islam, Mesoporous biopolymer architecture enhanced the adsorption and selectivity of aqueous heavy-metal ions, ACS Omega, 6 (2021) 15316–15331.
[32] X. Li, C. Zhu, G. Xu, X. Han, Removal of Pb(II) with amorphous titanium(IV) hydrogen phosphate loaded on SiO_2, Chin. J. Environ. Eng., 8 (2014) 1510–1514 (in Chinese).
[33] A. Demirbas, Heavy metal adsorption onto agro-based waste materials: a review, J. Hazard. Mater., 157 (2008) 220–229.
[34] J.X. Yu, L.Y. Wang, R.A. Chi, Y.F. Zhang, Z.G. Xu, J. Guo, Competitive adsorption of Pb^{2+} and Cd^{2+} on magnetic modified sugarcane bagasse prepared by two simple steps, Appl. Surf. Sci., 268 (2013) 163–170.
[35] H. Chen, J. Zhao, G. Dai, J. Wu, H. Yan, Adsorption characteristics of Pb(II) from aqueous solution onto a natural biosorbent, fallen *Cinnamomum camphora* leaves, Desalination, 262 (2010) 174–182.
[36] X. Xu, X. Cao, L. Zhao, H. Wang, H. Yu, B. Gao, Removal of Cu, Zn, and Cd from aqueous solutions by the dairy manure-derived biochar, Environ. Sci. Pollut. Res. Int., 20 (2013) 358–368.
[37] N. Zhao, B. Li, H.M. Huang, X.M. Lv, M.G. Zhang, L. Cao, Modification of kelp and sludge biochar by TMT-102 and NaOH for cadmium adsorption, J. Taiwan Inst. Chem. Eng., 116 (2020) 101–111.
[38] Y. Jin, M. Zhang, Z.H. Jin, G.L. Wang, R. Li, X. Zhang, X.S. Liu, J.J. Qu, H.M. Wang, Characterization of biochars derived from various spent mushroom substrates and evaluation of their adsorption performance of Cu(II) ions from aqueous solution, Environ. Res., 196 (2021) 1–14.
[39] P. Mondal, C.B. Majumder, B. Mohanty, Effects of adsorbent dose, its particle size and initial arsenic concentration on the removal of arsenic, iron and manganese from simulated ground water by Fe^{3+} impregnated activated carbon, J. Hazard. Mater., 150 (2008) 695–702.
[40] P. Zhang, O. David, Y. Wang, L. Jiang, T.X. Xia, L.W. Wang, C.W.T. Daniel, S.O. Yong, D.Y. Hou, A green biochar/iron oxide composite for methylene blue removal, J. Hazard. Mater., 384 (2020) 1–8.
[41] A.R. Lucaci, D. Bulgariu, I. Ahmad, G. Lisă, A.M. Mocanu, L. Bulgariu, Potential use of biochar from various waste biomass as biosorbent in Co(II) removal processes, Water, 11 (2019) 1–15.
[42] H. Jin, S. Capareda, Z. Chang, J. Gao, Y. Xu, J. Zhang, Biochar pyrolytically produced from municipal solid wastes for aqueous As(V) removal: adsorption property and its improvement with KOH activation, Bioresour. Technol., 169 (2014) 622–629.
[43] A.A. Adenuga, O.D. Amos, J.A.O. Oyekunle, E.H. Umukoro, Adsorption performance and mechanism of a low-cost biosorbent from spent seedcake of *Calophyllum inophyllum* in simultaneous cleanup of potentially toxic metals from industrial wastewater, J. Environ. Chem. Eng., 7 (2019) 1–9.
[44] I. Morosanu, C. Teodosiu, D. Fighir, C. Paduraru, Simultaneous biosorption of micropollutants from aqueous effluents by rapeseed waste, Process Saf. Environ. Prot., 132 (2019) 231–239.
[45] M. Pakdel, S. Soleimanian-Zad, S. Akbari-Alavijeh, Screening of lactic acid bacteria to detect potent biosorbents of lead and cadmium, Food Control, 100 (2019) 144–150.
[46] F.A. Tapouk, R. Nabizadeh, S. Nasseri, A. Mesdaghinia, H. Khorsandi, A.H. Mahvi, E. Gholibegloo, M. Alimohammadi, M. Khoobi, Endotoxin removal from aqueous solutions with dimethylamine-functionalized graphene oxide: modeling study and optimization of adsorption parameters, J. Hazard. Mater., 368 (2019) 163–177.
[47] P. Ndagijimana, X.J. Liu, Z.W. Li, G.W. Yu, Y. Wang, Optimized synthesis of a core-shell structure activated carbon and its adsorption performance for bisphenol A, Sci. Total Environ., 689 (2019) 457–468.
[48] Y.H. Wu, Y. Fan, M.L. Zhang, S.X. Yang, A. Arkin, P Fang, Functionalized agricultural biomass as a low-cost adsorbent: utilization of rice straw incorporated with amine groups for the adsorption of Cr(VI) and Ni(II) from single and binary systems, Biochem. Eng. J., 105 (2016) 27–35.
[49] E. Hodgson, A. Lewys-James, S.R. Ravella, S. Thomas-Jones, J. Gallagher, Optimisation of slow-pyrolysis process conditions to maximise char yield and heavy metal adsorption of biochar produced from different feedstocks, Bioresour. Technol., 214 (2016) 574–581.
[50] Ihsanullah, A. Abbas, A.M. Al-Amer, T. Laoui, M.A. Atieh, Heavy metal removal from aqueous solution by advanced carbon nanotubes: critical review of adsorption applications, Sep. Purif. Technol., 157 (2016) 141–161.
[51] Y.D. Chen, S.H. Ho, D. Wang, Z.S. Wei, J.S. Chang, N.Q. Ren, Lead removal by a magnetic biochar derived from persulfate-ZVI treated sludge together with one-pot pyrolysis, Bioresour. Technol., 247 (2017) 463–470.
[52] C. Nzediegwu, M.A. Naeth, S.X. Chang, Lead(II) adsorption on microwave-pyrolyzed biochars and hydrochars depends on feedstock type and production temperature, J. Hazard. Mater., 412 (2021) 1–12.
[53] L. Trakal, V. Veselská, I. Šafařík, M. Vítková, S. Číhalová, M. Komárek, Lead and cadmium sorption mechanisms on magnetically modified biochars, Bioresour. Technol., 203 (2016) 318–324.
[54] M.A.P. Cechinel, S.M.A.G. De-Souza, A.A.U. De-Souza, Study of lead(II) adsorption onto activated carbon originating from cow bone, J. Cleaner Prod., 65 (2014) 342–349.
[55] J.H. Kwak, M.S. Islam, S. Wang, S.A. Messele, M.A. Naeth, M.G. El-Din, S.X. Chang, Biochar properties and lead(II) adsorption capacity depend on feedstock type, pyrolysis temperature, and steam activation, Chemosphere, 231 (2019) 393–404.
[56] J. Shi, X. Fan, D.C.W. Tsang, F. Wang, Z. Shen, D. Hou, D.S. Alessi, Removal of lead by rice husk biochars produced at different temperatures and implications for their environmental utilizations, Chemosphere, 235 (2019) 825–831.
[57] Y.H. Li, S. Wang, J. Wei, X. Zhang, C. Xu, Z. Luan, D. Wu, B. Wei, Lead adsorption on carbon nanotubes, Chem. Phys. Lett., 357 (2002) 263–266.
[58] W. Chen, Z. Lu, B. Xiao, P. Gu, W. Yao, J. Xing, A.M. Asiri, K.A. Alamry, X Wang, S. Wang, Enhanced removal of lead ions from aqueous solution by iron oxide nanomaterials with cobalt and nickel doping, J. Cleaner Prod., 211 (2019) 1250–1258.
[59] K. Chen, J. He, Y. Li, X. Cai, K. Zhang, T. Liu, Y. Hu, D. Lin, L. Kong, J. Liu, Removal of cadmium and lead ions from water by sulfonated magnetic nanoparticle adsorbents, J. Colloid Interface, 494 (2017) 307–316.
[60] Z. Shi, C. Xu, H. Guan, L. Li, L. Fan, Y. Wang, L. Liu, Q. Meng, R. Zhang, Magnetic metal–organic frameworks (MOFs) composite for removal of lead and malachite green in wastewater, Colloids Surf., A, 539 (2017) 382–390.
[61] X. Du, M.J. Zhao, Z.C. Ma, S.T. Xing, Adsorption properties for Pb^{2+} removal onto biochars from different sources of biomass feedstock, J. Yanshan Univ., 40 (2016) 552–560 (in Chinese).
[62] Q. Zeng, S.X. Wang, L. Hu, H. Zhong, Z.G. He, W. Sun, D.L. Xiong, Oxalic acid modified copper tailings as an efficient adsorbent with super high capacities for the removal of Pb^{2+}, Chemosphere, 263 (2021) 127833, doi: 10.1016/j.chemosphere.2020.127833.
[63] T.A. Saleh, V.K. Gupta, Characterization of the chemical bonding between Al_2O_3 and nanotube in MWCNT/Al_2O_3 nanocomposite, Curr. Nanosci., 8 (2012) 739–743.
[64] M. Samimi, M. Shahriari-Moghadam, Isolation and identification of *Delftia lacustris* strain-MS3 as a novel and efficient adsorbent for lead biosorption: kinetics and thermodynamic studies, optimization of operating variables, Biochem. Eng. J., 173 (2021) 108091, doi: 10.1016/j.bej.2021.108091.